Journal of Materials Chemistry A

High Efficient Near-infrared and Semitransparent Polymer Solar Cells Based on an Ultra-Narrow Bandgap Nonfullerene Acceptor

Journal:	*Journal of Materials Chemistry A*
Manuscript ID	TA-ART-11-2018-011484.R2
Article Type:	Paper
Date Submitted by the Author:	10-Jan-2019
Complete List of Authors:	Chen, Juan; Soochow University, Chemical Engineering and Materials Science Li, Guangda; Soochow University Zhu, Qinglian; Xi'an Jiaotong University, State Key Laboratory for Mechanical Behavior of Materials Guo, Xia; Soochow University, Laboratory of Advanced Optoelectronic Materials, College of Chemistry, Chemical Engineering and Materials Science Fan, Qunping; Soochow University, Ma, Wei; Xi'an Jiaotong University, State Key Laboratory for Mechanical Behavior of Materials Zhang, Maojie; Soochow University, Laboratory of Advanced Optoelectronic Materials, College of Chemistry, Chemical Engineering and Materials Science

High Efficient Near-infrared and Semitransparent Polymer Solar Cells Based on an Ultra-Narrow Bandgap Nonfullerene Acceptor

Juan Chen,[‡a] Guangda Li,[‡a] Qinglian Zhu,[b] Xia Guo,*[a] Qunping Fan,[a] Wei Ma,[b] and Maojie Zhang*[a]

[a] State and Local Joint Engineering Laboratory for Novel Functional Polymeric Materials, Laboratory of Advanced Optoelectronic Materials, College of Chemistry, Chemical Engineering and Materials Science, Soochow University, Suzhou 215123, China

*E-mail: mjzhang@suda.edu.cn; guoxia@suda.edu.cn

[b] State Key Laboratory for Mechanical Behavior of Materials, Xi'an Jiaotong University, Xi'an 710049, China

[‡] These authors contributed equally to this work.

Abstract: In this work, we design and synthesize an acceptor-donor-acceptor structured non-fullerene acceptor (ACS8) with an ultra-narrow bandgap (1.3 eV). It possesses well-ordered molecular orientation and π-π stacking, and hence exhibits a high electron mobility of 2.65×10^{-4} cm^2 V^{-1} s^{-1}. The polymer solar cells (PSCs) based on PTB7-Th:ACS8 (1:2, w/w) processed by toluene with 0.5% PN (1-phenylnaphthalene) treatment exhibited an optimal power conversion efficiency (PCE) of 13.2% with an open circuit voltage (V_{oc}) of 0.75 V, a short-circuit current density (J_{sc}) of 25.3 mA cm^{-2} and a fill factor (FF) of 69.3% under the illumination of AM 1.5G, 100 mW cm^{-2}. This PCE is among the highest values reported in the literatures to date for the PSCs based on ultra-narrow bandgap acceptors ($E_g^{opt} \leq 1.3$ eV). Furthermore, semitransparent devices based on PTB7-Th:ACS8 exhibit an outstanding PCE up to 11.1% with the average visible transmittance of 28.6%.

Keywords: non-fullerene acceptor; polymer solar cells; alkylthio substituents; PN additive.

1. Introduction

Polymer solar cells (PSCs) as a promising renewable energy technology have attracted great attention due to their unique advantages, such as light weight, low cost, easy fabrication and capability to be fabricated into large area and flexible devices through roll-to-roll processing.[1-5] In typical bulk heterojunction (BHJ) PSCs, the active layer is generally comprised of a p-type conjugated polymer as the donor and a n-type organic semiconductor (n-OS) as the acceptor. In comparison with the fullerenes, non-fullerene (NF) n-OS acceptors have exhibited great potential for high efficient PSCs due to their distinguished advantages of easily tunable optical absorption and electronic energy levels, low production cost and good morphology stability.[6-15] Therefore, the NF-PSCs have drawn considerable attention and made great progress in recent years with the power conversion efficiencies (PCEs) up to 11-14% for single-junction devices[16-25] and 14-17% for tandem devices[26-30].

Among the NF n-OS acceptors, the fused-ring electron acceptors (FREAs) with an acceptor-donor-acceptor (A-D-A) structure based on fused aromatic cores with strong electron withdrawing groups[31-40], such as ITIC,[31] IDIC,[32] IT-4F,[33] ATT-1,[38] NFBDT,[40] have become dominant in highly efficient PSCs. These acceptors exhibits a strong absorption in the wavelength of 500-800 nm with the optical bandgap (E_g^{opt}) over 1.5 eV. When blended with wide bandgap polymer donors with complementary absorption and matched energy levels, the devices can sufficiently utilized the visible light and the best PCE over 14% have been achieved.[41-43] Considering the trade-off between the open circuit voltage (V_{oc}) and the bandgap, it is a great challenge to further improve the performance of single-junction devices limited by the absorption in the near-infrared (NIR) region and unavoidable energy loss ($E_{loss}=E_g^{opt}-eV_{oc}$). However, the exploitation of ultra-narrow bandgap non-fullerene acceptor (NFA, $E_g^{opt} \leq 1.3$ eV) with high V_{oc} and external quantum efficiency (EQE) in NIR is rather rare and has impeded the progress of the tandem devices.[27,29] For example, although the

representative ultra-narrow bandgap NFA, IEICO-4F, exhibited an ultra-narrow bandgap of 1.24 eV, the device based on the blend of PTB7-Th and IEICO-4F only exhibited a medium PCE of ~12%.[44,45] In addition, as one of unique advantages of PSCs, semitransparent (ST) devices have great potential for use in building integrated photovoltaics (BIPV) and power generating windows.[46-52] Recently, the ST-PSCs based on the NFAs have exhibited an outstanding PCE of 10.2 % with an average visible transmittance (AVT) of 31%.[53] However, the lack of NIR acceptors also restrain to achieve high efficient and high transparent ST-PSCs. Hence, to develop a new NIR NFA is an urgent issue for the PSCs application.

In this work, we designed and synthesized a small molecule acceptor ACS8 with indacenodithiophene (IDT) as core, alkylthio-substituted thiophene as π-bridge and electron-withdrawing 3-(1,1-dicyanomethylene)-5,6-difluoro-1-indanone (IC2F) as end groups (as shown in Fig. 1a). ACS8 film shows a narrow-bandgap of 1.3 eV with strong absorption in the region of 650-900 nm, and a redshift of 80 nm compared with that in solution. Moreover, ACS8 film possesses well-ordered molecular orientation and π-π stacking, and hence exhibited a high electron mobility of 2.65×10^{-4} cm^2 V^{-1} s^{-1}. The PSCs based on PTB7-Th:ACS8 (1:2, w/w) with 0.5% PN (1-phenylnaphthalene) exhibited an optimal PCE of 13.2% with a V_{oc} of 0.75 V, a short-circuit current density (J_{sc}) of 25.3 mA cm^{-2} and a fill factor (FF) of 69.3% under the illumination of AM 1.5G, 100 mW cm^{-2}. This PCE is the highest value reported in the literatures to date for the PSCs based on NIR acceptors ($E_g^{opt} \leq$ 1.3 eV). Furthermore, semitransparent devices based on PTB7-Th:ACS8 (1:2, w/w) exhibited PCEs varying from 9.4% to 11.1% at different AVT (43.2-28.6%). These results indicate that ACS8 is a very promising NIR acceptor material for semitransparent and tandem solar cells applications.

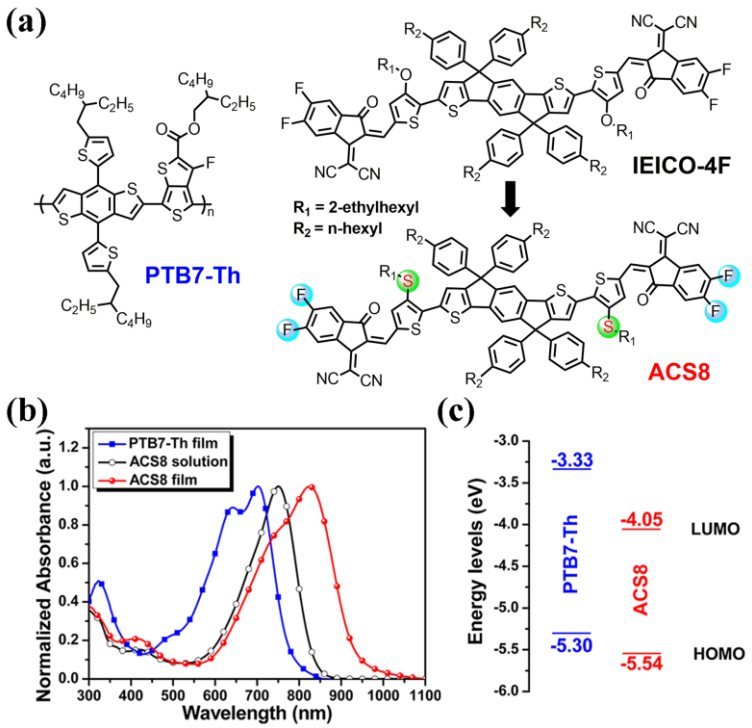

Fig. 1. (a) Molecular structures of ACS8, IEICO-4F and PTB7-Th, (b) UV-Vis absorption spectra of ACS8 in CF solution and ACS8 and PTB7-Th in films, and (c) molecular energy level diagrams of PTB7-Th and ACS8.

2. Results and Discussion

The synthetic routes and molecular structure of ACS8 are shown in Scheme S1 and Fig. 1a, respectively. The detailed synthesis and characterization data are provided in the Supporting Information. ACS8 has been characterized by ^{1}H NMR, ^{13}C NMR and Matrix-Assisted Laser Desorption/Ionization Time of Flight Spectrometry (MALDI-TOF MS). ACS8 shows good solubility in common organic solvents, such as chloroform (CF), chlorobenzene (CB) and toluene (TL) at room temperature. Moreover, ACS8 exhibits a decomposition temperature (Td) of 334 °C at 5% weight loss as shown in the thermogravimetric analysis (TGA) plot in Fig. S1, which indicates that it has good thermal stability for application in PSCs.

As shown in Fig. 1b, ACS8 in solution exhibits an absorption in the region of 600-850

nm with the maximum absorption peak (λ_{max}) at 751 nm. In the thin film, the absorption peak redshifts ca. 80 nm compared with that in solution, which should be attributed to the strong aggregation of molecule chain in the solid state. The E_g^{opt} of ACS8 estimated from the absorption edge (λ_{edge}= 950 nm) of the thin film is 1.30 eV with an increase of 0.06 eV in comparison with that of IEICO-4F (1.24 eV)[44]. Furthermore, the electron mobility of ACS8 was evaluated by the space-charge-limited current method (Fig. S8) and a higher value of 2.65×10^{-4} cm^2 V^{-1} s^{-1} was achieved than that of IEICO-4F (1.14×10^{-4} cm^2 V^{-1} s^{-1}).

The electrochemical property of ACS8 was investigated by cyclic voltammetry (CV). As shown in Fig. 1c and Fig. S2, the highest occupied molecular orbital (HOMO) and the lowest unoccupied molecular orbital (LUMO) energy levels of ACS8 estimated from the onset oxidation potential (φ_{ox}) and reduction potential (φ_{red}) are -5.54 eV and -4.05 eV, respectively. Hence, ACS8 exhibits a lower HOMO and a similar LUMO relative to IEICO-4F (HOMO= -5.46 eV; LUMO= -4.08 eV). Moreover, theoretical calculations are performed by using the density functional theory (DFT) to investigate the influence of alkoxyl and alkylthiol on the properties of the small molecule acceptors as show in Fig. S3. There are no obvious differences for ACS8 and IEICO-4F in their optimized molecular conformations and the electron distributions of the frontier molecular orbitals. In comparison with IEICO-4F, ACS8 shows a similar LUMO and a downshifted HOMO, which is consistent with the CV measurement results.

To investigate the photovoltaic properties of ACS8, the PSCs with an inverted structure of ITO/ZnO/poly[(9,9-bis(3′-(N,N-dimethylamino)propyl)-2,7-fluorene)-alt-2,7-(9,9-dioctylfluorene)] (PFN)/PTB7-Th:ACS8/MoO_3/Al were fabricated using TL as the host processing solvent. Firstly, the influence of D/A weight ratio of the blend active layer was investigated. As shown in Fig. S4 and Table S1, the optimal D/A weight ratio was 1:2 (w/w), and a PCE of 9.8% was obtained with a V_{oc} of 0.75 V, a J_{sc} of 22.1 mA cm^{-2} and an FF of

58.8%. In order to further improve the photovoltaic performance, PN was utilized as solvent additive to optimize the morphology of the active layers as shown in Fig. S5 and Table S2. Fig. 2a-b shows the current density-voltage (*J*-*V*) characteristics and EQE curves of the solar cells based on the PTB7-Th:ACS8 without and with 0.5% PN. It was found that using PN as solvent additive can remarkably improve the PCEs of the devices due to the significantly enhanced J_{sc} and FF. Furthermore, when 0.5% PN was added, the devices exhibited the best PCE of 13.2% with a V_{oc} of 0.75 V, a J_{sc} of 25.3 mA cm^{-2} and an FF of 69.3% . Moreover, under the same device processing conditions, the devices based on IEICO-4F just exhibited a moderate PCE of 9.4% (Fig. S6). To our knowledge, the PCE of 13.2 % is the highest value reported in the literatures to date for the PSCs based on NIR acceptors ($E_g^{opt} \leq 1.3$ eV).[41,45] As shown in Fig. 2b, when adding 0.5% PN as solvent additive, the EQE curves was signicifantly enhanced and redshifted in the long wavelength region of 600-900nm. Moreover, a maximum EQE value of 82.6% at 650 nm was recorded for the optimal device. The integrated J_{sc} from the EQE curves were 21.3 and 24.2 mA cm^{-2} for the PSCs based on the blend film without and with 0.5% PN treatment, respectively, which agrees well with the *J*-*V* measurements. The variations of EQE and J_{sc} should be related to the absorption and carrier mobilities of the blend films. As shown in Fig. S7, the absorption spectrum of the blend film with PN treatment exhibited an obvious redshift and an enhanced absorption peak in the long wavelength, which is in agreement with the EQE curves. As shown in Fig. S8 and Table S3, the hole/electron mobilities (μ_h/μ_e) were estimated to be 1.47/1.30 × 10^{-4} and 2.25/2.01 × 10^{-4} cm^2 V^{-1} s^{-1} for the blend film without and with 0.5% PN treatment, respectively. The higher and more balanced carrier mobilities for the blend film are beneficial to suppress space charge accumulation and promote the charge transport and extraction.

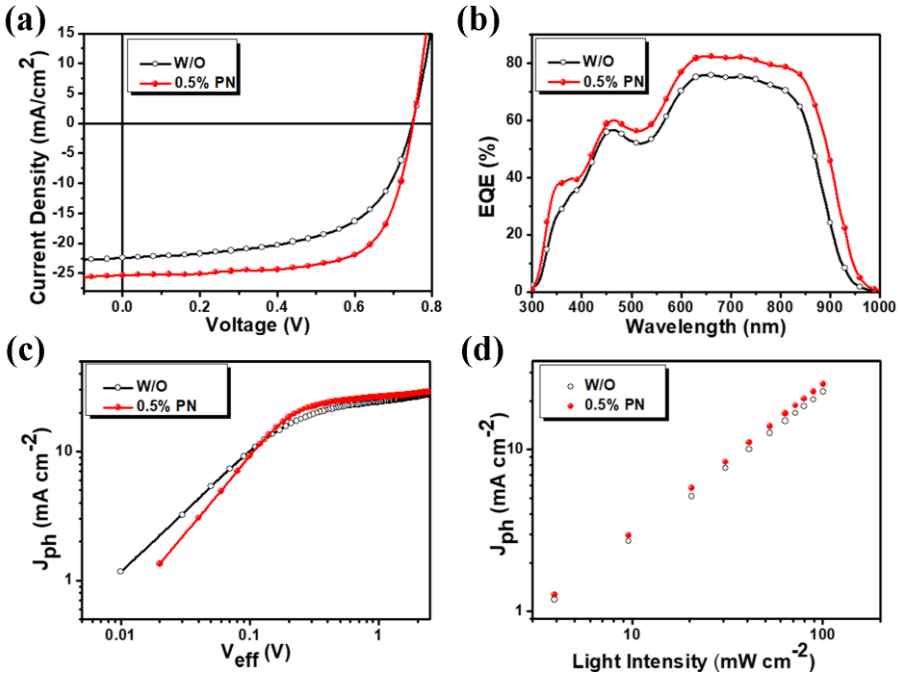

Fig. 2. (a) *J-V* characteristics, (b) EQE curves, (c) J_{ph} versus V_{eff} characteristics, and (d) dependence of J_{ph} on light intensity for the PSCs based on PTB7-Th:ACS8 (1:2, w/w) without or with 0.5% PN.

Table 1. Photovoltaic parameters of PSCs based on PTB7-Th:ACS8 (1:2, w/w) without PN or with 0.5% PN under the illumination of AM 1.5G, 100 mW cm^{-2}.

Conditions	V_{oc} (V)	J_{sc}[a] (mA cm^{-2})	FF (%)	PCE[b] (%)	Thickness (nm)
As-cast	0.75	22.5(21.3)	58.8	9.9 (9.7±0.2)	115
0.5% PN	0.75	25.3(24.2)	69.3	13.2 (13.1±0.1)	115

[a] Values calculated from EQE in brackets. [b] Average PCEs in brackets for over 30 devices.

As shown in Fig. 2c, the dependence of the photocurrent (J_{ph}) on the effective voltage (V_{eff}) was measured to investigate the impact of adding solvent additive on the exciton dissociation and charge collection process for PSCs. Here, J_{ph} is defined as J_L-J_D, where J_L and J_D are the current densities under illumination and in the dark, respectively. V_{eff} is

defined as V_0-V, where V_0 is the voltage at which the photocurrent is zero and V is the applied voltage.[54] The J_{ph} reaches the saturation current density (J_{sat}) at high V_{eff} ($\geq$ 2 V in this case). Thus, the exciton dissociation probability ($P(E, T)$) is determined from the ratio of J_{ph}/J_{sat}. Under maximal power output and short-circuit conditions, the values of $P(E, T)$ are 67.3/89.8% for the as-cast device, and 75.0/92.6% for the device with 0.5% PN treatment, respectively. The higher $P(E, T)$ indicates that solvent additive treatment leads to more efficient exciton dissociation and charge extraction efficencies, which is consistent with the better performance of the corresponding devices. Furtheremore, in oder to investigate the charge recombination process in the devices, the dependence of J_{ph} under different light intensities (P) was measured as shown in Fig. 2d. The relationship between J_{ph} and P is defined as $J_{ph} \propto P^S$. Weak bimolecular recombination in the device would result in a linear dependence of J_{ph} on P with S value close to 1.[55] The S values of the PSCs based on the blend without and with 0.5% PN are 0.92 and 0.93, respectively, implying the additive treatment has negligible effect on the biomolecualr recombination process in this blend.

Grazing incidence wide-angle X-ray scattering (GIWAXS) was performed to probe the effect of PN additive treatment on the molecular orientation and packing of the blend films.[56] Fig. 3a-b shows the 2D GIWAXS patterns and the corresponding scattering profiles in the in-plane (IP) and out-of-plane (OOP) direction. For the pure ACS8 film, the IP direction shows obvious (100) diffraction peak at 0.30 $Å^{-1}$ with a d-spacing of 20.73 Å, whereas the OOP shows a sharper and stronger peak at 1.79 $Å^{-1}$, corresponding to the (010) π-π staking with a d-spacing of 3.51 Å, indicating that the pure ACS8 film exhibits a dominated face-on molecular orientation relative to the substrate. The lamellar (100) diffraction peak of PTB7-Th film is located at 0.26 $Å^{-1}$ with a d-spacing of 24.02 Å in the IP direction. In as-cast PTB7-Th:ACS8 film, there is no apparent change at the lamellar (010) diffraction peak compared with the pure films, which is located at 1.79 $Å^{-1}$ for ACS8 and 1.57 $Å^{-1}$ for PTB7-

Th in the OOP direction, respectively. When adding PN additive, the blend film shows a stronger and tighter (100) diffraction peak and (010) diffraction peak at 0.31 and 1.80 $Å^{-1}$ respectively, corresponding to smaller lamellar distance of 20.00 and 3.50 Å respectively. The improved π-π staking ordering and enhanced face-on π-π stacking can be clearly observed after PN additive treatment, which is favorable for charge transport and thus obtaining high J_{sc} and FF. At the same time, we calculated the coherence length (CL) of π-π staking, which was calculated from the full width at half maximum (FWHM) of OOP using Scherrer equation.[57] Moreover, in the OOP direction, PTB7-Th: ACS8 film blend with PN additive treatment shows a larger CL of 10.11 nm compared to as-cast film blend with a CL of 3.97 nm, which means the overall crystallinity of the ACS8 was enhanced with PN additive treatment. Obviously, appropriate PN additive treatment promotes high crystalline behavior of the blend film and strong face-on orientation, which are desirable to vertical charge transport, thereby higher J_{sc} and FF.

The resonant soft X-ray scattering (R-SoXS) was used to probe the phase separation and average domain purity in PTB7-Th:ACS8 blend films.[58] The resonant photon energy of 284.8 eV was selected, where the material contrast dominates the scattering.[59] The PTB7-Th:ACS8 blend film without PN shows scattering peaks at q~0.096 nm^{-1}, corresponding to the domain size of ≈32 nm. The scattering peak of PTB7-Th:ACS8 blend film with 0.5% PN locates at q~0.083 nm^{-1}, corresponding to the domain size of ≈38 nm, which is slightly larger than the as-cast blend films. Moreover, as shown in Fig. 3c, the relative domain purity of the blends without and with PN additive treatment are 74% and 100%, respectively. The purer domains can reduce bimolecular recombination and thus lead to high performance. In a word, the appropriate domain sizes and the purer domains are beneficial to exciton dissociation and charge transport.[60] As a result, the devices based on PTB7-Th:ACS8 with 0.5% PN show higher J_{sc}, FF, and PCE.

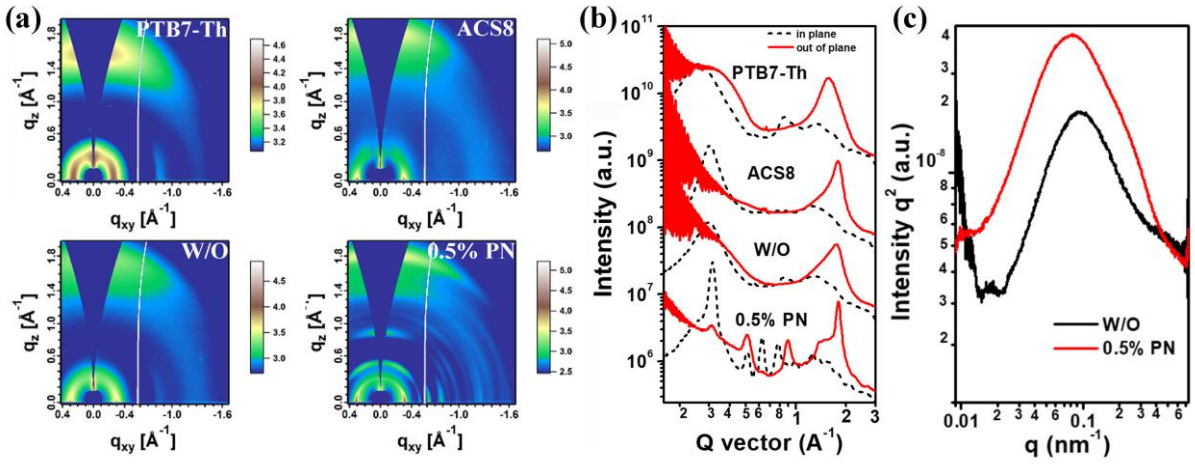

Fig. 3. (a) 2D GIWAXS patterns, (b) scattering profiles for pure films of ACS8, PTB7-Th and blend films of PTB7-Th: ACS8 (1:2, w/w) without PN or 0.5% PN and (c) R-SoXS profiles for PTB7-Th: ACS8 (1:2, w/w) blend films without PN or with 0.5% PN.

The surface and bulk morphologies of BHJ-films were probed using atomic force microscopy (AFM) and transmission electron microscopy (TEM). As shown in Fig. S9, the blend film with 0.5% PN treatment exhibits a relatively smooth surface with a root-mean-square (RMS) roughness of 1.03 nm in comparison with the as-cast blend film with RMS value of 1.26 nm. Moreover, as shown in Fig. S9f, when using the 0.5% PN as solvent additive, the phase separation and domain sizes of the blend film have been effectively optimized and the clear needle crystals of the ASC8 can be observed, which are beneficial for the exciton separation and charge transport.

Considering the blend of PTB7-Th:ASC8 shows a weak absorption in the region of 400-600 nm, the ST-PSCs with the structure of ITO/ZnO/PFN/PTB7-Th:ACS8/MoO_3/Au/Ag were fabricated. The ultrathin Au (1 nm) was used to reduce percolation of Ag film and enhance the Ag film uniformity, leading to optimal transmittance and low electrical resistance.[61] The *J-V* characteristics, EQE curves and transmission spectra are shown in Fig. 4a-c, and the corresponding photovoltaic parameters of the optimized devices summarized in Table 2. The photovoltaic performances of the devices with different Ag thickness (10 nm, 15 nm and 20

nm) were investigated. An obvious trade-off between the AVT and the PCE could be observed when changing the Ag thickness. When 10 nm Ag was used, the device showed good AVT of 43.2 % with a PCE of 9.4% and J_{sc} of 19.9 mA cm^{-2}. When the Ag thickness was increased to 20 nm, the AVT decreased to 28.6 % with a PCE of 11.1% and J_{sc} of 22.5 mA cm^{-1}, which are among the highest values for the ST-PSCs reported in the literatures.[20,47,52,62] The Comission Internationale de I'Eclairage (CIE) 1931 color coordinate of the transmitted light under CIE standard illuminant D65 (Fig. 4d), correlated color temperature (CCT) and coloring rendering index (CRI) of the ST devices are summarized in Table 2. The champion ST-PSCs with a 20 nm Ag show a CIE of (0.2621,0.2976) close to the white color point (1/3,1/3), demonstrating their good neutral color feature and possess a CCT of 11528K and a CRI of 84.

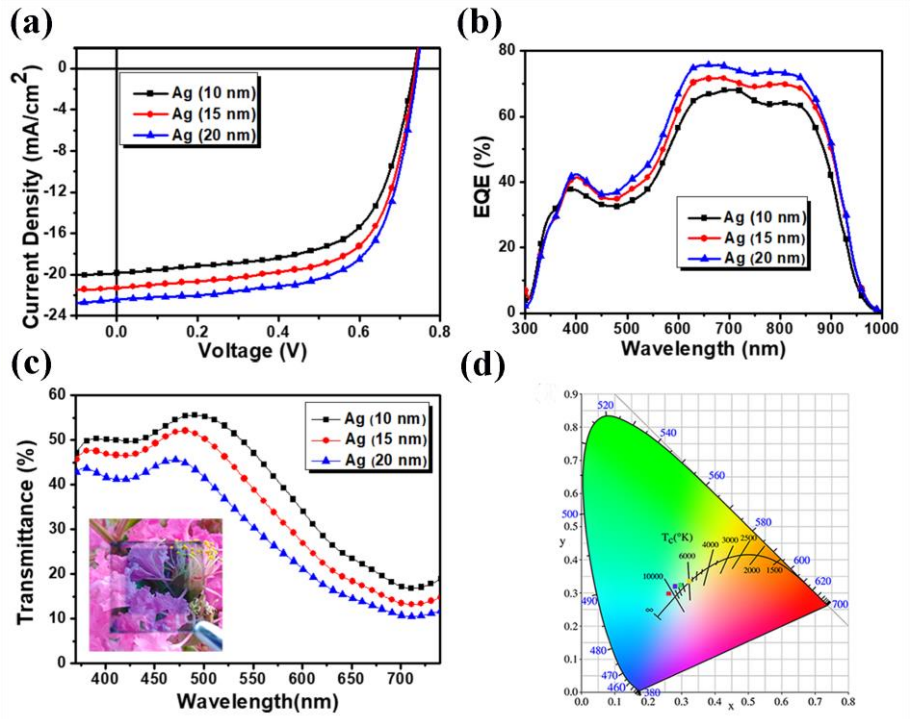

Fig. 4. (a)The *J-V* characteristics, (b) the corresponding EQE curves of the ST-PSCs based on PTB7-Th:ACS8 (1:2, w/w) with different Ag thickness, (c) transmittance spectra of the ST-OSC with different Ag thicknesses (the inset graph is a photo of the semitrasparent device with a 10 nm thick Ag) and (d) the representation of color coordinates of the semitransparent

devices with different Ag thickness (10 nm, red dot; 15 nm, blue dot and 20 nm, green dot) on CIE.

Table 2. Photovoltaic parameters of the ST-PSCs based on PTB7-Th:ACS8 (1:2, w/w) with different Ag thickness under the illumination of AM 1.5G, 100 mw/cm^2.

Ag thickness (nm)	AVT (%)	CIE coordinate	CCT (k)	CRI	V_{oc} (V)	J_{sc}[a] (mA cm^{-2})	FF (%)	PCE[b] (%)
10	43.2	(0.2958, 0.3239)	7547	91	0.74	19.9 (18.9)	63.8	9.4 (9.3±0.1)
15	36.1	(0.2808, 0.3201)	8665	86	0.74	21.3 (20.2)	65.7	10.4 (10.2±0.2)
20	28.6	(0.2621, 0.2976)	11528	84	0.74	22.5 (21.3)	66.5	11.1 (11.0±0.1)

[a] Values calculated from EQE in brackets. [b] Average PCEs in brackets for over 30 devices.

3. Conclusions

In summary, a new small molecule acceptor (ACS8) based on IDT as core, alkylthio-substituted thiophene as π-bridge and electron-withdrawing IC2F as end groups has been designed and synthesized for PSCs applications. ACS8 shows a narrow-bandgap of 1.30 eV with strong absorption in the region of 650-900 nm and a relatively low LUMO energy level of -4.05 eV. Furthermore, ACS8 film possesses well-ordered molecular orientation and tightly face-on packing, and hence exhibits a high electron mobility of 2.65×10^{-4} cm^2 V^{-1} s^{-1}. The PSCs based on PTB7-Th:ACS8 (1:2, w/w) with 0.5% PN exhibited an optimal PCE of 13.2% with a V_{oc} of 0.75 V, a J_{sc} of 25.3 mA cm^{-2} and an FF of 69.3% under the illumination of AM 1.5G, 100 mW cm^{-2}. Furthermore, semitransparent devices based on PTB7-Th: ACS8 (1:2,

w/w) exhibited PCEs varying from 9.4% to 11.1% at different AVT (43.2-28.6%). These results indicate that ACS8 is a very promising NIR acceptor material for semitransparent and tandem solar cells applications.

Acknowledgements

J. Chen and G.D. Li contributed equally to this work.This work was supported by National Natural Science Foundation of China (NSFC) (No. 51573120, 51503135, 51773142, 21704082, 21875182 and 91633301), Ministry of science and technology (No. 2016YFA0200700), China Postdoctoral Science Foundation (2017M623162). The X-ray data was acquired at beamlines 7.3.3 and 11.0.1.2 at the Advanced Light Source, which is supported by the Director, Office of Science, Office of Basic Energy Sciences, of the U.S. Department of Energy under Contract No. DE-AC02-05CH11231. The authors thank Chenhui Zhu at beamline 7.3.3, and Cheng Wang at beamline 11.0.1.2 for assistance with data acquisition.

References

1. Y. F. Li, *Acc. Chem. Res.* 2011, **45**, 723.
2. J. W. Chen, Y. Cao, *Acc. Chem. Res*. 2009, **42**, 1709.
3. G. Li, R. Zhu, Y. Yang, *Nat. Photonics*. 2012, **6**, 153.
4. S. M. Ryno, M. K. Ravva, X. K. Chen, H. Y. Li, J. L. Brédas, *Adv. Energy Mater*. 2016, **6**, 1601370.
5. C. J. Brabec, M. Heeney, I. McCulloch, J. Nelson, *Chem. Soc. Rev*. 2011, **40**, 1185.
6. J. Hou, O. Inganas, R. H. Friend, F. Gao, *Nat. Mater*. 2018, **17**, 119.
7. W. Li, H. Yao, H. Zhang, S. Li, J. Hou, *Chem-Asian. J*. 2017, **12**, 2160.
8. R. Yu, H. Yao, J. Hou, *Adv. Energy Mater*. 2018, **8**, 1702814.
9. P. Cheng, G. Li, X. Zhan, Y. Yang, *Nat. Photonics*. 2018, **12**, 131.
10. B. Fan, L. Ying, Z. Wang, B. He, X. F. Jiang, F. Huang, Y. Cao, *Energy Environ. Sci*.

2017, **10**, 1243.

11. Y. Lin, X. Zhan, Acc. *Chem. Res*. 2016, **49**, 175.
12. Y. Lin, Y. Li, X. Zhan, *Chem. Soc. Rev*. 2012, **41**, 4245.
13. Y. Lin, X. Zhan, *Mater. Horiz.* 2014, **1**, 470.
14. X. Zhan, A. Facchetti, S. Barlow, T. J. Marks, M. A. Ratner, M. R. Wasielewski, S. R. Marder, *Adv. Mater*. 2011, **23**, 268.
15. V. A. Trukhanov, D. Y. Paraschuk, *Polym. Sci. Ser. C*. 2014, **56**, 72.
16. H. Yao, L. Ye, J. Hou, B. Jang, G. Han, Y. Cui, G. M. Su, C. Wang, B. Gao, R. Yu, H. Zhang, Y. Yi, H. Y. Woo, H. Ade, J. Hou, *Adv. Mater.* 2017, **29**, 1700254.
17. Z. Xiao, X. Jia, D. Li, S. Wang, X. Geng, F. Liu, J. Chen, S. Yang, T. P. Russell, L. Ding, *Sci. Bull*. 2017, **62**, 1494.
18. J. Wang, W. Wang, X. Wang, Y. Wu, Q. Zhang, C. Yan, W. Ma, W. You, X. Zhan, *Adv. Mater*. 2017, **29**, 1702125.
19. S. Li, L. Ye, W. Zhao, X. Liu, J. Zhu, H. Ade, J. Hou, *Adv. Mater.* 2017, **29**, 1704051.
20. J. Wang, J. Zhang, Y. Xiao, T. Xiao, R. Zhu, C. Yan, Y. Fu, G. Lu, X. Lu, S. R. Marder, X. Zhan, *J. Am. Chem. Soc*. 2018, **140**, 9140.
21. J. Sun, X. Ma, Z. Zhang, J. Yu, J. Zhou, X. Yin, L. Yang, R. Geng, R. Zhu, F. Zhang, W. Tang, *Adv. Mater.* 2018, **30**, 1707150.
22. W. Gao, M. Zhang, T. Liu, R. Ming, Q. An, K. Wu, D. Xie, Z. Luo, C. Zhong, F. Liu, F. Zhang, H. Yan, C. Yang, *Adv. Mater.* 2018, **30**, 1800052.
23. S. J. Xu, Z. Zhou, W. Liu, Z. Zhang, F. Liu, H. Yan, X. Zhu, *Adv. Mater.* 2017, **29**, 1704510.
24. J. Zhu, Z. Ke, Q. Zhang, J. Wang, S. Dai, Y. Wu, Y. Xu, Y. Lin, W. Ma, W. You, X. Zhan, *Adv. Mater.* 2017, **30**, 1704713.
25. (a) Y. Yang, Z. G. Zhang, H. Bin, S. Chen, L. Gao, L. Xue, C. Yang, Y. Li, *J. Am. Chem.*

Soc. 2016, **138**, 15011; (b) C. Li, T. Xia, J. Song, H. Fu, H. Ryu, K. Weng, L. Ye H. Y. Woo, Y. Sun, *J. Mater. Chem. A.* 2018, DOI:10.1039/C8TA11197A.

26. Y. Zhang, B. Kan, Y. Sun, Y. Wang, R. Xia, X. Ke, Y. Q. Yi, C. Li, H. L. Yip, X. Wan, Y. Cao, Y. Chen, *Adv. Mater.* 2018, **30**, 1707508.
27. L. X. Meng, Y. M. Zhang, X. J. Wan, C. X. Li, X. Zhang, Y. B. Wang, X. Ke, Z. Xiao, L. M. Ding, R. X. Xia, H. L. Yip, Y. Cao, Y. S. Chen, *Science.* 2018. **361**, 1094.
28. Y. Cui, H. Yao, B. Gao, Y. Qin, S. Zhang, B. Yang, C. He, B. Xu, J. Hou, *J. Am. Chem. Soc*. 2017, **139**, 7302.
29. Y. Cui, H. F. Yao, C. Y. Yang, S. Q. Zhang, J. H. Hou, *Acta Polym. Sin*. 2018, **2**, 223.
30. X. Che, Y. Li, Y. Qu, S. R. Forrest, *Nat. Energy*. 2018, **3**, 422.
31. Y. Lin, J. Wang, Z. G. Zhang, H. Bai, Y. Li, D. Zhu, X. Zhan, *Adv. Mater.* 2015, **27**, 1170.
32. Y. Lin, Q. He, F. Zhao, L. Huo, J. Mai, X. Lu, C. J. Su, T. Li, J. Wang, J. Zhu, Y. Sun, C. Wang, X. Zhan, *J. Am. Chem. Soc*. 2016, **138**, 2973.
33. W. Zhao, S. Li, H. Yao, S. Zhang, Y. Zhang, B. Yang, J. Hou, *J. Am. Chem. Soc*. 2017, **139**, 7148.
34. Y. Lin, F. Zhao, Q. He, L. Huo, Y. Wu, T. C. Parker, W. Ma, Y. Sun, C. Wang, D. Zhu, A. J. Heeger, S. R. Marder, X. Zhan, *J. Am. Chem. Soc*. 2016, **138**, 4955.
35. Y. Lin, Z.-G. Zhang, H. Bai, J. Wang, Y. Yao, Y. Li, D. Zhu, X. Zhan, *Energy Environ. Sci.* 2015, **8**, 610.
36. (a) Z. Zhang, L. Feng, S. Xu, J. Yuan, Z. G. Zhang, H. Peng, Y. Li, Y. Zou, *J. Mater. Chem. A.* 2017, **5**, 11286; (b) G. Zhang, G. Yang, H. Yan, J. H. Kim, H. Ade, W. Wu, X. Xu, Y. Duan, Q. Peng, *Adv. Mater*. 2017, **29**, 1606054.
37. (a) Y. Li, D. Qian, L. Zhong, J.-D. Lin, Z. Q. Jiang, Z. G. Zhang, Z. Zhang, Y. Li, L. S. Liao, F. Zhang, *Nat. Energy.* 2016, **27**, 430; (b) B. Xiao, A. L. Tang, J. Q. Zhang, A.

Mahmood, Z. X. Wei, E. J. Zhou, *Adv. Energy Mater.* 2017, **7**, 1602269.

38. F. Liu, Z. Zhou, C. Zhang, T. Vergote, H. Fan, F. Liu, X. Zhu, *J. Am. Chem. Soc*. 2016, **138**, 15523.
39. (a) Y. Liu, Z. Zhang, S. Feng, M. Li, L. Wu, R. Hou, X. Xu, X. Chen, Z. Bo, *J. Am. Chem. Soc.* 2017, **139**, 3356; (b) Y. Chen, T. Liu, H. Hu, T. Ma, J. Y. L. Lai, J. Zhang, H. Ade and H. Yan, *Adv. Energy Mater.* 2018, **8**, 1801203.
40. B. Kan, H. Feng, X. Wan, F. Liu, X. Ke, Y. Wang, Y. Wang, H. Zhang, C. Li, J. Hou and Y. Chen, *J Am Chem Soc*. 2017, **139**, 4929.
41. B. Kan, H. Feng, H. Yao, M. Chang, X. Wan, C. Li, J. Hou, Y. Chen, *Sci. China Chem*. 2018, **61**, 1307.
42. Z. Zheng, Q. Hu, S. Zhang, D. Zhang, J. Wang, S. Xie, R. Wang, Y. Qin, W. Li, L. Hong, N. Liang, F. Liu, Y. Zhang, Z. Wei, Z. Tang, T. P. Russell, J. Hou, H. Zhou, *Adv. Mater.* 2018, **30**, 1801801.
43. S. Zhang, Y. Qin, J. Zhu, J. Hou, *Adv. Mater.* 2018, **30**, 1800868.
44. H. F. Yao, Y. C. R. N. Yu, B. W. Gao, H. Zhang, J. H. Hou, *Angew. Chem. Int. Ed.* 2017, **56**, 3045.
45. X. Song, N. Gasparini, L. Ye, H. F. Yao, J. H. Hou, H. Ade, D. Baran, *ACS Energy Lett.* 2018. **3**, 669.
46. C. J. Traverse, R. Pandey, M. C. Barr, R. R. Lunt, *Nat. Energy*. 2017, **2**, 849.
47. Y. Xie, L. Huo, B. Fan, H. Fu, Y. Cai, L. Zhang, Z. Li, Y. Wang, W. Ma, Y. Chen, Y. Sun, *Adv. Funct.Mater.* 2018, 1800627.
48. M. Zhang, X. Guo, W. Ma, H. Ade, J. Hou, *Adv. Mater.* 2015, **27**, 4655.
49. Y. Li, G. Xu, C. Cui, Y. Li, *Adv. Energy Mater.* 2018, **8**, 1701791.
50. Y. Li, J. D. Lin, X. Che, Y. Qu, F. Liu, L. S. Liao, S. R. Forrest, *J. Am. Chem. Soc*. 2017, **139**, 17114.

51. S. Dai, X. Zhan, *Adv. Energy Mater.* 2018, **8**, 1800002.

52. F. Liu, Z. Zhou, C. Zhang, J. Zhang, Q. Hu, T. Vergote, F. Liu, T. P. Russell, X. Zhu, *Adv. Mater.* 2017, **29**,1606574.

53. B. Jia, S. Dai, Z. Ke, C. Yan, W. Ma, X. Zhan, *Chem. Mater.* 2017, **30**, 239.

54. J. L. Wu, F. C. Chen, Y. S. Hsiao, F. C. Chien, P. Chen, C. H. Kuo, M. H. Huang, C. S. Hsu, *ACS. Nano.* 2011, **5**, 959.

55. P. W. M. Blom, V. D. Mihailetchi, L. J. A. Koster, D. E. Markov, *Adv. Mater*. 2007, **19**, 1551.

56. A. Hexemer, W. Bras, J. Glossinger, E. Schaible, E. Gann, R. Kirian, A. MacDowell, M. Church, B. Rude, H. Padmore, *J. Phys. Conf. Ser.* 2010, **247**, 012007.

57. S. J. Ko, W. Lee, H. Choi, B. Walker, S. Yum, S. Kim, T. J. Shin, H. Y. Woo, J. Y. Kim, *Adv. Energy Mater.* 2015, **5**, 1401687.

58. Y. Wu, Z. Y. Wang, X. Y. Meng, W, *Prog. Chem.* 2017, **29**, 93.

59. E. Gann, A. T. Young, B. A. Collins, H. Yan, J. Nasiatka, H. A. Padmore, H. Ade, A. Hexemer, C. Wang, *Rev. Sci. Instrum.* 2012, **83**, 045110.

60. H. B. Naveed, W. Ma, *Joule*. 2018, **2**, 621.

61. S. Schubert, J. Meiss, L. Müller-Meskamp, K. Leo, *Adv. Energy Mater*. 2013, **3**, 438.

62. W. Wang, C. Yan, T. K. Lau, J. Wang, K. Liu, Y. Fan, X. Lu, X. Zhan, *Adv. Mater.* 2017, **29**, 1701308.

The table of contents entry

The non-fullerene polymer solar cells based on a low bandgap polymer PTB7-Th and a ultra-narrow bandgap acceptor ACS8 exhibited optimal PCE of 13.2%, indicating that the blend of PTB7-Th/ACS8 is potential for the practical applcation of PSCs.

Keywords: non-fullerene acceptor; polymer solar cells; alkylthio substituents; PN additive.

High Efficient Near-infrared and Semitransparent Polymer Solar Cells Based on an Ultra-Narrow Bandgap Nonfullerene Acceptor

Juan Chen, Guangda Li, Qinglian Zhu, Xia Guo, Qunping Fan, Wei Ma, and Maojie Zhang*